

Line of Sight Bias in Dark Matter Inferences from Galaxy Cluster Mergers

DAVID WITTMAN¹ AND SCOTT ADLER¹

¹*Department of Physics and Astronomy, University of California, Davis, CA 95616 USA*

ABSTRACT

In collisions of galaxy clusters, the lack of displacement between dark matter and galaxies suggests that the dark matter scattering depth is small. This yields an upper limit on the dark matter cross section if the dark matter column density is known. We investigate a bias in such constraints: the measured column density (along the line of sight, using gravitational lensing) is lower than that experienced by a dark matter particle, as follows. Dark matter halos are triaxial and generally collide along their major axes, yielding a high scattering column density—but the merger is obvious only to observers whose line of sight is nearly perpendicular to that axis, yielding a low observed column density. We trace lines of sight through merging halos from the BigMDPL n-body simulation, both with and without mock observational effects. We find that a hypothetical skewer through the halo along the merger axis (more precisely, along the current separation vector of the two halos) has twice the column density of a typical line of sight. With weak lensing measurements, which involve some spatial averaging, this ratio is reduced to 1.25, suggesting that existing constraints on the scattering cross section are biased high by about 25%.

Keywords: Galaxy clusters (584); dark matter (353)

1. INTRODUCTION

Dark matter (DM) is the dominant form of matter in the universe, but little is known about its particle properties. One key question is to what extent, if any, DM particles can scatter off each other. The astrophysical effects of such scattering, also known as self-interacting dark matter (SIDM), were first discussed by Spergel & Steinhardt (2000), who also presented rough upper limits on the scattering cross section per unit mass $\frac{\sigma_{\text{DM}}}{m}$ based on those effects. In many particle models, $\frac{\sigma_{\text{DM}}}{m}$ will be velocity-dependent, so constraints from different astrophysical environments should be considered in the context of the typical particle velocity in that environment (Kaplinghat et al. 2016). The highest velocities probed are in the mergers of galaxy clusters, with relative speeds of ~ 3000 km/s (Markevitch et al. 2004; Randall et al. 2008; Harvey et al. 2015; Robertson et al. 2017; Wittman et al. 2018b).

Markevitch et al. (2004) identified the Bullet cluster as a post-pericenter snapshot of a nearly head-on collision between two galaxy clusters. A hallmark of recent pericenter passage is a substantial separation between gas and galaxies (later called *dissociation* by Dawson et al. (2011)) due to momentum exchange between the gas distributions around the time of pericenter. (Markevitch et al. 2004) argued that the *lack* of separation be-

tween DM and galaxies implied that the DM scattering depth $\tau = \frac{\sigma_{\text{DM}}}{m} \Sigma < 1$, where Σ is the surface mass density encountered by a DM particle of one halo as it passes through the other halo. Hence Σ^{-1} yields an upper limit on $\frac{\sigma_{\text{DM}}}{m}$ if no significant galaxy-DM separation is observed. Harvey et al. (2014) generalized this argument to yield an estimate of $\frac{\sigma_{\text{DM}}}{m}$ if a separation is observed.

This paper explores a bias in this method. In practice Σ is measured along the line of sight (LOS), but for purposes of the DM constraint it should be measured along the merger trajectory, or along the current separation vector (CSV) as a proxy. Because halos are triaxial (Jing & Suto 2002) and preferentially aligned with neighboring halos (Binggeli 1982; Plionis 1994; Kasun & Evrard 2005; Smargon et al. 2012), the surface mass density probed along the CSV, Σ_{CSV} , will tend to be larger than the surface mass density probed along a random LOS, Σ_{LOS} . Furthermore, the merging systems used for these constraints tend to be those in which the LOS is perpendicular to the CSV, such that physical separations would be visible as angular separations. This implies that Σ_{LOS} is measured along a triaxial halo’s intermediate or minor axis, biasing it low compared to a random LOS. If the ratio $\frac{\Sigma_{\text{LOS}}}{\Sigma_{\text{CSV}}} < 1$, then the DM scattering depth is underestimated and $\frac{\sigma_{\text{DM}}}{m}$ is overestimated. This paper examines dark matter-only n-body

simulations to quantify the factor by which $\frac{\sigma_{DM}}{m}$ is overestimated.

In §2 we describe our methods, in §3 we present the results, and in §4 we discuss the impact of the results.

2. METHODS

We approximate each halo as a triaxial ellipsoid, meaning that its density ρ is a function only of the scaled radial coordinate $R \equiv \sqrt{(\frac{x}{a})^2 + (\frac{y}{b})^2 + (\frac{z}{c})^2}$ where a , b , and c denote the semiaxis lengths ($a > b > c$). We assume for notational simplicity here a Cartesian coordinate system aligned with the halo principal axes; in practice, this can be achieved by a rotation from the coordinate system of the simulation in which the halo is embedded. Given this functional form, the surface mass density Σ along any skewer piercing the ellipsoid can be expressed as the skewer distance across the ellipsoid times an integral $\int_0^\infty \rho(R)dR$ that depends *only* on the density profile. Therefore the ratio $\frac{\Sigma_{los}}{\Sigma_{CSV}}$ cancels the latter factor and involves only the ratio of distances across the ellipsoid. This skewer ratio is informative, so we present some results in those terms. But in practice, densities are not measured along an arbitrarily thin geometric line; they are measured by gravitational lensing, which averages over a large patch of sky. We quantify this effect with mock weak lensing analyses described near the end of this section.

2.1. Geometric definitions

Figure 1 illustrates the geometry used in this paper. The black arrow defines the first principal axis (major axis) of the triaxial halo, while the red arrow shows an illustrative CSV (the other halo involved in the merger is not shown). Halos tend to be aligned with their neighbors, so the angle ψ is generally small as shown. The LOS is drawn at a larger angle α from the separation vector, because lines of sight near the separation vector would not identify a merger as dissociative. There are techniques for constraining α (e.g., Wittman et al. 2018a) but these do not constrain the relationship between the LOS and the halo principal axes. Hence, the LOS could be anywhere along a cone with opening angle α . Figure 1 shows two possible LOS along this cone, illustrating that one involves a considerably longer path through the halo hence a larger Σ_{los} .

We calculate the distance through the halo along the CSV, and along all possible LOS (at a given α) to obtain a distribution for $\frac{\Sigma_{los}}{\Sigma_{CSV}}$ given a specific halo, merger, and α . We can then marginalize over many halos and mergers to obtain a distribution for $\frac{\Sigma_{los}}{\Sigma_{CSV}}$ given α . The selection of mergers could be tailored to match a specific observed system as in Wittman (2019), but this paper derives results for mergers in general.

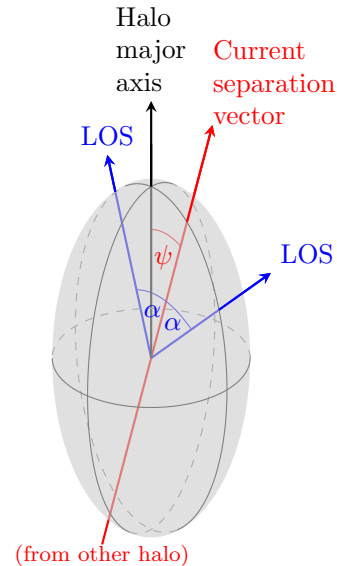


Figure 1. Definition of angles. ψ is subtended by the halo major axis and the current separation vector to the other halo in the merger (not shown here). Lines of sight (LOS) fall along a cone defined by the separation vector and α .

2.2. Simulation inputs and calculations

We used the publicly available Big Multidark Planck (BigMDPL, Klypin et al. 2016) simulation hosted on the CosmoSim¹ website (Riebe et al. 2013). This dark matter simulation has a very large box size, $(2.5 \text{ Gpc}/h)^3$, which maximizes the number of merging halo pairs. The mass of each particle in the simulation is $2.359 \times 10^{10} M_\odot$, so even the least massive clusters considered here ($M > 6 \times 10^{13} M_\odot$) have over 250 particles. The Λ CDM cosmological parameters were set to $h = 0.6777$, $\Omega_\Lambda = 0.692885$, and $\Omega_m = 0.307115$.

We use the catalog of halo pairs assembled in Wittman et al. (2018a) and Wittman (2019). Briefly, this is derived from the BigMDPL Rockstar (Behroozi et al. 2013) halo catalog by finding halo pairs that have passed exactly one pericenter (within 300 kpc). This is in principle a different catalog at each snapshot, but we focus on one illustrative snapshot (number 74, $z = 0.1058$). We discarded halo pairs with current separations < 0.25 Mpc, as these were too overlapping for Rockstar to derive robust shape parameters. Observed mergers with current separations < 0.25 Mpc are also rare because they are observationally difficult to disentangle.

We use the `axis1_[xyz]` attributes (square brackets denote use of each enclosed letter) to determine the orientation of the halo major axis. The orientations of the second and third principal axis are not documented, so

¹ <https://www.cosmosim.org/metadata/bigmdpl/>

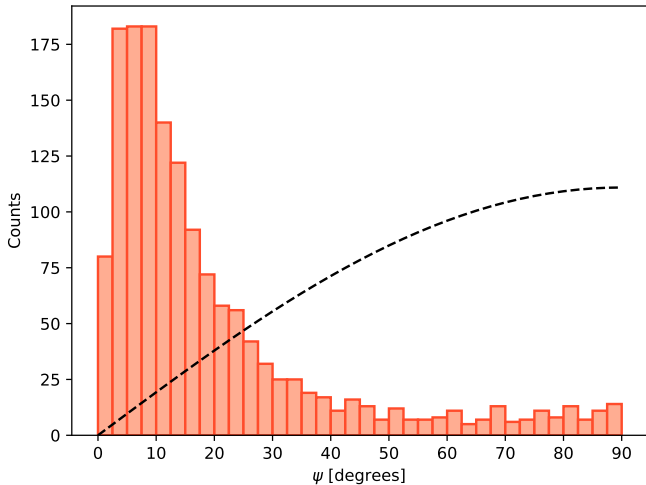


Figure 2. Histogram of the angle ψ between the merger axis and each halo’s major axis. The two axes show a remarkable tendency for alignment (small ψ), in contrast to the dashed curve which shows the distribution expected for ψ distributed randomly on a sphere.

we marginalize over them as described below. We used the `axisratio_[23]_1` attributes to quantify the axis ratios. For a given halo, we first compute the angle ψ between the halo’s major axis and the CSV given by the halo-pair catalog; see Figure 1. We then calculate the skewer lengths (hence $\frac{\Sigma_{\text{los}}}{\Sigma_{\text{CSV}}}$) for a variety of LOS, and finally group the skewer results by the angle α between the CSV and the LOS.

For weak lensing estimates, we use analytical formulae (Heyrovský & Karamazov 2024) for the reduced shear field around a triaxial NFW Navarro et al. (1997) profile to generate mock weak-lensing data. We then fit the mock shear field, with a spherical NFW model, as is typically done in the observational literature. We then tabulate the ratio of inferred mass using a given LOS to that using the CSV.

3. RESULTS

3.1. Halo-merger alignment

Figure 2 shows the alignment between the CSV and each halo’s major axis, in terms of a histogram of the angle ψ . The two axes show a remarkable tendency for alignment (small ψ), in contrast to the dashed curve which shows the distribution expected for CSVs randomly distributed on a sphere. Assuming the clusters fell toward each other along a connecting filament, this is consistent with work finding that cluster-scale halos are aligned along larger-scale filaments, which aligns them with neighboring halos (Kasun & Evrard 2005).

For binary merging clusters specifically, we would expect good halo-halo alignment because both halos are falling toward each other along a filament with which

they are each aligned. We are not aware of empirical measurements of this effect, which may be difficult given overlapping halos. However, halo-halo alignment in binary mergers can be inferred from two empirical results: the orientation of a brightest cluster galaxy (BCG) is a proxy for the orientation of its host cluster (West et al. 2017), and BCGs in merging clusters are known to align with the CSV (Wittman et al. 2019).

3.2. Skewer surface mass density

Illustrative halos. Figure 3, top panel, shows the results for an illustrative halo ($\psi = 1.5^\circ$, $\frac{b}{a} = 0.337$, $\frac{c}{a} = 0.259$). Results are shown as violin plots for values of α in 5° increments. At $\alpha = 0$, $\frac{\Sigma_{\text{los}}}{\Sigma_{\text{CSV}}} = 1$ by definition and only one LOS is sampled so no violin appears. As α increases, the the LOS pierces the halo closer to the intermediate or minor axis, so $\frac{\Sigma_{\text{los}}}{\Sigma_{\text{CSV}}}$ falls below unity. Furthermore, at each $\alpha > 0$ there are multiple LOS, yielding a range of $\frac{\Sigma_{\text{los}}}{\Sigma_{\text{CSV}}}$ depending on their proximity to the halo minor or intermediate axis. Observed systems are typically identified as mergers and used for DM constraints only if $\alpha > 45^\circ$, so this halo suggests that $\frac{\Sigma_{\text{los}}}{\Sigma_{\text{CSV}}} \approx 0.3$. In other words, the surface mass density encountered by DM particles through the pericenter passage is about three times that measured along the LOS, so the resultant DM constraint would be biased high by a factor of three.

Figure 3, bottom panel, shows a halo with matching axis ratios but with $\psi = 18^\circ$ misalignment from the CSV. Therefore the maximum Σ_{los} is encountered by one LOS at $\alpha = 18^\circ$: the LOS that happens to align with the major axis. Other LOS at $\alpha = 18^\circ$ encounter a range of lower column densities. As one proceeds to higher α the LOS are sampling the intermediate and minor axes—but to a lesser degree than with a well-aligned halo, hence Σ_{los} does not drop as far.

All halos. A few halo pairs provided remarkably large or small bias factors, for example when one halo’s major axis points at the other’s minor axis in a “T” shape. We suspect that these extreme cases are artifacts of the halo finder having difficulty separating overlapping halos. To reduce clutter from these possibly unphysical cases, in Figure 4 we show the median and interquartile range (IQR) of the bias factor distribution after marginalizing over all halos in the relevant halo pairs. Again, considering that observed cases will have $\alpha > 45^\circ$, the surface mass density encountered by DM particles through the pericenter passage is nearly twice that measured along the LOS, so the resultant DM constraint would be biased high by a factor of nearly two.

Effect of mass. Figure 5 shows how these trends differ across halo mass quartiles; for clarity only the median

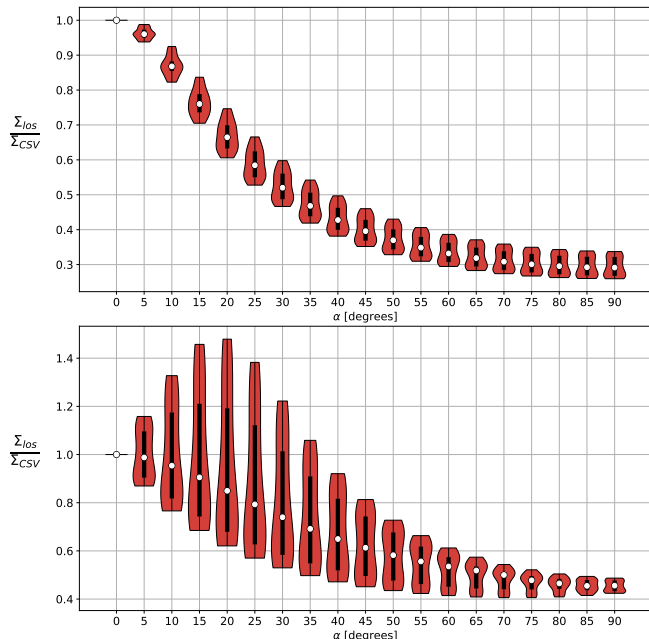


Figure 3. Skewer bias factor $\frac{\Sigma_{\text{los}}}{\Sigma_{\text{CSV}}}$ as a function of viewing angle α for two halos with similar axis ratios. Top: halo 13410052637 is well aligned with its merger axis ($\psi = 1.5^\circ$), such that lines of sight perpendicular to the merger axis (large α) encounter systematically low column density. Bottom: halo 13582533817 is less well aligned ($\psi = 18^\circ$), leading to more mixed results but still with bias at large α . In each case the violin shows the distribution, which the open circle marks the median and the black band marks the middle quartiles.

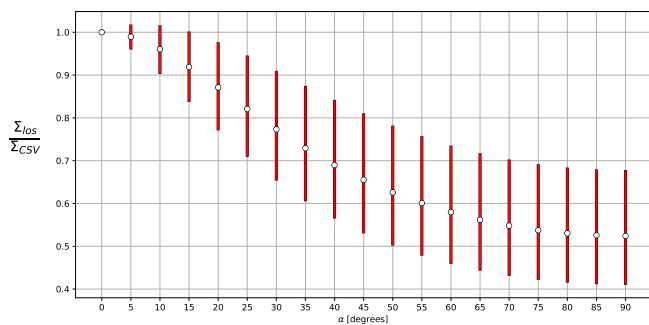


Figure 4. Median (circles) and interquartile range (bars) of the skewer bias factor marginalized over all halos, as a function of viewing angle α . For typical observed cases $\alpha > 45^\circ$ so the surface mass density along the LOS is about half that encountered by DM particles along the separation vector. At face value, this implies an overestimate of DM cross sections by a factor of two.

effect at each α and mass bin is shown. Lower-mass halos are rounder (in BigMDPL as well as in other works, e.g. Allgood et al. 2006; Henson et al. 2016) so the effects of LOS are less marked at lower mass.

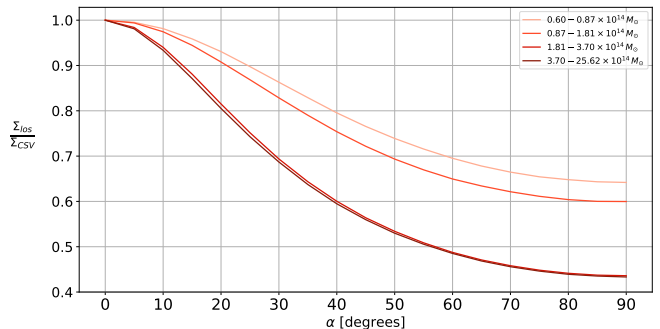


Figure 5. Median skewer bias factor $\frac{\Sigma_{\text{los}}}{\Sigma_{\text{CSV}}}$ as a function of viewing angle α , marginalized over all halos in a given mass quartile. Lower-mass halos show reduced LOS effects because they are rounder.

3.3. Mock weak lensing results

The skewer results presented so far represent a hypothetical measurement with unlimited angular resolution. Weak lensing (WL) involves a larger footprint on the sky so may be less sensitive to LOS. Our mock WL results confirm that, for a given halo and LOS pair, the mass ratio between the two LOS is less extreme for WL than for the skewer. At the largest α , where a skewer along the LOS measures only half the surface density of a skewer along the CSV, we find that the WL ratio is 0.8. This more modest sensitivity to LOS is consistent with Euclid Collaboration et al. (2024) who performed mock WL fits along the principal axes of clusters in the Three Hundred simulation (Cui et al. 2018) and found that orientations along the (major, intermediate, minor) axes bias the inference of the true mass by factors of about (1.2, 0.85, 0.75).²

We show these results as a function of α in Figure 6. Again, the ratio is normalized to unity at $\alpha = 0$, where there is a single LOS. At other α the median and interquartile range are shown, illustrating the variation across halos and LOS (e.g. LOS perpendicular to the major axis still sample a range from the minor to the intermediate axis). The full distribution is omitted for clarity. For large α the bias factor is just above 0.8.

Figure 7 shows the same results split by mass quartile. For small to moderate α , the WL results are consistent with the skewer results: low-mass halos are rounder so are less sensitive to LOS effects. However, at large α the low-mass halos actually exhibit more bias. The mechanism for this is unclear, as there are many steps in the WL fitting process. However, the pattern is consistent with Figure 10 of Euclid Collaboration et al.

² The Three Hundred halos include baryons so should be slightly rounder than our BigMDPL halos which are dark matter only. However, this is a small effect; see §4.

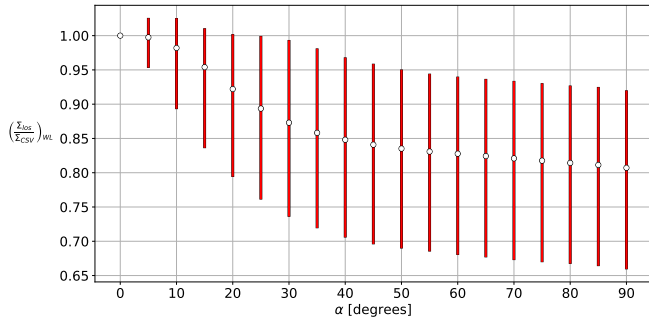


Figure 6. Weak lensing bias factor as a function of viewing angle α , marginalized over all halos. The circles indicate medians and the bars indicate the interquartile range. The trend is the same as for skewer measures of column density, but the bias factor is less extreme.

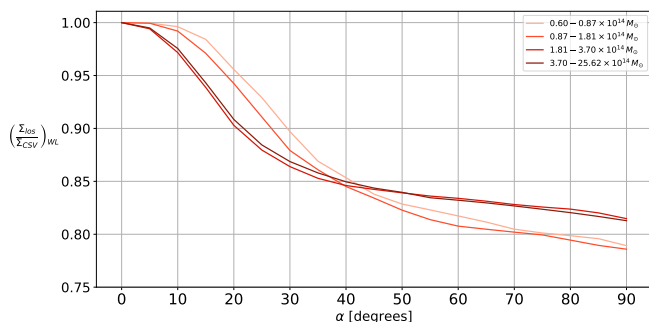


Figure 7. Median weak lensing bias factor as a function of viewing angle α , marginalized over all halos in a given mass quartile.

(2024), which found the inferred WL mass increasing more quickly with true mass when viewed along the intermediate and minor axes than when viewed along the major axis. In either case there is a great deal of scatter from halo to halo, so this trend is not highly significant.

4. SUMMARY AND DISCUSSION

We have found that current $\frac{\sigma_{\text{DM}}}{m}$ constraints based on the scattering depth argument are on average biased because spherical symmetry is violated: the surface mass density along the LOS is lower than that experienced by DM particles as they pass along the merger axis. Because the surface mass density is inversely related to the inferred cross section, this yields an overestimate of the DM cross section—by a factor of ≈ 2 for surface mass densities measured along skewers (infinitesimally narrow paths through a halo). This bias is reduced to ≈ 1.25 for weak lensing mass measurements, which average sources over a large patch of sky. Note that this bias is distinct from the overall mass bias studied in Lee et al. (2023), which is smaller and stems from the overlap of two hypothetically spherical halos.

We studied dark matter only (DMO) halos; the presence of baryons will reduce bias by making halos rounder, but only slightly. For example, the simulations of Henson et al. (2016) found that the minor/major axis ratio shifts from 0.537 for DMO to 0.576 with baryons. This is only 40% of the scatter across halos. The intermediate/major axis ratio shifts by a similarly small amount when baryons are added.

The bias is a function of halo and LOS properties, so more precise estimates could in principle be tailored to each individual observed system. Such tailoring would involve a straightforward extension of the procedure here: rather than counting all halo pairs with equal weight in the marginalization, one should weight by the likelihood of a halo pair matching the observables (subhalo projected separation, mass, and line-of-sight relative velocity).

Most known binary systems were identified due to their clear separation between subclusters on the sky, hence α is not small. This is why we have referred to lines of sight at large α as “typical.” This is likely to remain the case for any cluster amenable to this DM scattering argument; for mergers along the LOS there is no mechanism for measuring a DM offset.

Although our argument was framed in terms of analytical approximations relating $\frac{\sigma_{\text{DM}}}{m}$ to scattering depth (Markevitch et al. 2004; Harvey et al. 2014), the same bias applies to staged simulations based on the assumption of spherical symmetry. To overcome this bias, staged simulations should be staged with appropriate halo shapes and alignments, and we urge simulators to do so. A further step would be to go beyond the triaxial approximation and resimulate merging systems found in cosmological simulations. This would incorporate the effect of finer substructure and the fact that axis ratios vary with density (Jing & Suto 2002). Resimulating appropriate boxes chosen from cosmological simulations would also naturally incorporate the appropriate range of halo alignments and pericenter distances.

ACKNOWLEDGMENTS

We thank Rodrigo Stancioli for constructive suggestions. This work was supported by NSF grant number 2308383. The CosmoSim database used in this paper is a service by the Leibniz-Institute for Astrophysics Potsdam (AIP). The MultiDark database was developed in cooperation with the Spanish MultiDark Consolider Project CSD2009-00064. The authors gratefully acknowledge the Gauss Centre for Supercomputing e.V. (www.gauss-centre.eu) and the Partnership for Advanced Supercomputing in Europe (PRACE, www.prace-ri.eu) for funding the MultiDark simulation project by providing computing time on the GCS Supercomputer SuperMUC at Leibniz Supercomputing Centre (LRZ, www.lrz.de).

REFERENCES

- Allgood, B., Flores, R. A., Primack, J. R., et al. 2006, *MNRAS*, 367, 1781
- Behroozi, P. S., Wechsler, R. H., & Wu, H.-Y. 2013, *ApJ*, 762, 109
- Binggeli, B. 1982, *A&A*, 107, 338
- Cui, W., Knebe, A., Yepes, G., et al. 2018, *MNRAS*, 480, 2898
- Dawson, W. A., Wittman, D., Jee, M., et al. 2011, *ArXiv e-prints*, arXiv:1110.4391
- Euclid Collaboration, Giocoli, C., Meneghetti, M., et al. 2024, *A&A*, 681, A67
- Harvey, D., Massey, R., Kitching, T., Taylor, A., & Tittley, E. 2015, *Science*, 347, 1462
- Harvey, D., Tittley, E., Massey, R., et al. 2014, *MNRAS*, 441, 404
- Henson, M. A., Barnes, D. J., Kay, S. T., McCarthy, I. G., & Schaye, J. 2016, *Monthly Notices of the Royal Astronomical Society*, 465, 3361
- Heyrovský, D., & Karamazov, M. 2024, *arXiv e-prints*, arXiv:2404.00169
- Jing, Y. P., & Suto, Y. 2002, *ApJ*, 574, 538
- Kaplinghat, M., Tulin, S., & Yu, H.-B. 2016, *PhRvL*, 116, 041302
- Kasun, S. F., & Evrard, A. E. 2005, *The Astrophysical Journal*, 629, 781
- Klypin, A., Yepes, G., Gottlöber, S., Prada, F., & Heß, S. 2016, *MNRAS*, 457, 4340
- Lee, W., Cha, S., Jee, M. J., et al. 2023, *ApJ*, 945, 71
- Markevitch, M., Gonzalez, A. H., Clowe, D., et al. 2004, *ApJ*, 606, 819
- Navarro, J. F., Frenk, C. S., & White, S. D. M. 1997, *ApJ*, 490, 493
- Plionis, M. 1994, *ApJS*, 95, 401
- Randall, S. W., Markevitch, M., Clowe, D., Gonzalez, A. H., & Bradač, M. 2008, *ApJ*, 679, 1173
- Riebe, K., Partl, A. M., Enke, H., et al. 2013, *Astronomische Nachrichten*, 334, 691
- Robertson, A., Massey, R., & Eke, V. 2017, *MNRAS*, 465, 569
- Smargon, A., Mandelbaum, R., Bahcall, N., & Niederste-Ostholt, M. 2012, *MNRAS*, 423, 856
- Spergel, D. N., & Steinhardt, P. J. 2000, *Phys. Rev. Lett.*, 84, 3760
- West, M. J., de Propris, R., Bremer, M. N., & Phillipps, S. 2017, *Nature Astronomy*, 1, 0157
- Wittman, D. 2019, *ApJ*, 881, 121
- Wittman, D., Cornell, B. H., & Nguyen, J. 2018a, *ApJ*, 862, 160
- Wittman, D., Foote, D., & Golovich, N. 2019, *ApJ*, 874, 84
- Wittman, D., Golovich, N., & Dawson, W. A. 2018b, *ApJ*, 869, 104